

Electronic Supplementary Information (ESI)

Remarkable sorption properties of polyamide 12 microspheres for a broad-spectrum antibacterial (triclosan) in water

Jie Han,^{*a} Zhi Cao^b and Wei Gao^a

^aDepartment of Chemical and Materials Engineering, The University of Auckland, 20 Symonds Street, Auckland 1010, New Zealand.

^bDepartment of Chemistry, Purdue University, 560 Oval Drive, West Lafayette, IN 47907, USA.

Table of Contents

1.	Experimental methods
	Sorbent materials and characterization
	Sorption isotherm, kinetics and selectivity
	Sorbent regeneration
	Analytical method
	Computational chemistry calculations
2.	Description of the isotherm and kinetics models used in this study
	Langmuir and Freundlich isotherm models
	Pseudo-second-order kinetics model
3.	Figures
Fig. S1	Typical morphologies of PA12 microspheres observed under a scanned electron microscope
Fig. S2	TCS molecular geometry computed by MARVIN® 5.9.3 Suite. Image displays the lowest energy conformer of TCS molecule.
Fig. S3	Sorption isotherm of TCS on PA12, AC and PS-DVB in aqueous solutions. Data are fitted to Freundlich and Langmuir isotherm models. Sorbent dosage: 10 mg (dry weight basis), 200 mL; agitation: 225 rpm, 48 h; at 298 K. C_e (mg L ⁻¹) represents TCS equilibrium concentration and q_e (mg g ⁻¹) represents the corresponding sorption capacity.
Fig. S4	Structures and atomic charges of amide groups in <i>N</i> -methylacetamide (NMA) and aliphatic polyamides (APA)
Fig. S5	Sorption isotherms of TCS on PA6 and PA12 microspheres in aqueous solutions. Sorbent dosage: 10 mg (dry weight basis), 200 mL; agitation: 225 rpm, 48 h; at 298 K.
Fig. S6	Structural formula and atom numbering schemes of TCS, TCS-methyl and phenol molecules (above); chemical repeating unit in PA6 and PA12 (below).
Fig. S7	Sorption kinetics of TCS by PA12, AC and PS-DVB in aqueous solutions. Sorption data are fitted to the pseudo second-order kinetics model. Initial TCS concentration: 1.0 mg L ⁻¹ ; sorbent dosage: 100 mg (dry weight basis), 500 mL; agitation: 225 rpm; at 298 K.
Fig. S8	Sorbent regeneration via hydrothermal treatment, alkaline elution and solvent elution
Fig. S9	Microspecies distribution of TCS solutes in water at different pH levels as predicted by calculations using MARVIN® 5.9.3 Suite
4.	Tables
Table S1	ATR-FTIR spectrum of PA12 microspheres and comparison with standard PA12 spectral data
Table S2	Comparison with relevant literature data on the sorption capacity for TCS in water
Table S3	Quantum mechanical modeling of the bond distances and energies of intermolecular hydrogen bonds in a ternary system consisting of NMA, TCS and H ₂ O molecules
Table S4	Effects of water chemistry constituents on the sorption of TCS by PA12, AC and PS-DVB
Table S5	Physicochemical properties of sorbent materials
5.	References

^{*} Corresponding author. Present address: NSF STC WaterCAMPWS, Dept. of Civil and Environmental Engineering, University of Illinois at Urbana-Champaign, 205 North Mathews Ave., Urbana, IL 61801, USA. Tel: 1 217 333 8038; Fax: 1 217 333 9464; E-mail: jiehan2@illinois.edu

1. Experimental methods

Sorbent materials and characterization. The physicochemical properties of sorbent materials are shown in Table S5. PA12 (Arkema Inc., France) was supplied as nonporous spherical microspheres with a mean size of $5 \pm 1 \mu\text{m}$ and a specific surface area of $9.1 \text{ m}^2 \text{ g}^{-1}$. A commonly used AC sorbent (Norit® 1240W, Norit Netherlands B.V.) and a macroreticular PS-DVB adsorbent resin (AMBERLITE™ XAD4, Dow Chemical Co., USA), were used as benchmark sorbents in this study. PA12 microspheres were rinsed in acetone (Scharlau Chemie S.A.) and $18.2 \text{ M}\Omega\text{-cm}$ deionized water (Milli-Q), and dried in vacuum at 303 K for 24 h before use. The moisture content of PS-DVB resin was verified by drying 3 samples in vacuum overnight at 303 K and measuring the weight differences. ATR-FTIR spectra of PA12 microspheres were recorded on a Perkin-Elmer Spectrum 1000 FTIR spectrometer. Sample scanning was performed at a resolution of 4 cm^{-1} with a minimum of 4 scans for each sample. The spectral data was acquired by the Spectrum™ 6.3.1 program. Specific surface areas were determined by N_2 adsorption isotherms using a Micromeritics TriStar 3000 system. Samples were degassed at 343 K in vacuum before adsorption measurements. The specific surface areas and pore volumes of sorbents were determined from the N_2 adsorption data using the BET method.

Sorption isotherm, kinetics and selectivity. Agitated batch sorption experiments were conducted to establish the sorption isotherm of TCS on each sorbent. Each batch used a series of 200 mL TCS (Irgasan®, $\geq 97\%$, HPLC grade, Sigma) solutions with a range of initial concentrations and a constant dosage of 10 mg sorbents on a dry weight basis. Due to the low aqueous solubility of TCS ($\leq 10 \text{ mg L}^{-1}$) and high sorption capacities of the sorbents used, the sorbent dosage was optimized to obtain a gradient of TCS equilibrium concentrations after sorption equilibrium. Each batch of sorbent-containing solutions was agitated at 225 rpm for 48 h in an incubator shaker to reach equilibrium at 298 K. The agitation speed was carefully selected to maintain the fluidization of AC and PS-DVB particles in the solution with no attrition-induced particle breakage after 48 h of agitation. After the equilibrating period, sample were extracted from the solutions and filtered by $0.2\text{-}\mu\text{m}$ pore size regenerated cellulose (RC) membrane filters (13 mm dia., Phenomenex) for chromatography analysis.

The sorption kinetics of TCS by PA12, PS-DVB and AC sorbents was studied by dosing 100 mg sorbents into 500 mL TCS solution (1.0 mg L^{-1}) and monitoring the time profile of free TCS concentrations in the agitated solution. Samples were collected at pre-set time intervals and each sample was filtered immediately after extraction. The sorption behavior of TCS, TCS-methyl (analytical standard, Fluka) and phenol ($\geq 99\%$, Aldrich) was comparatively studied on the three sorbents. Sorption equilibrium was obtained by dosing 100 mg sorbents into 500 mL sorbate compound solution (TCS and phenol: $3.45 \mu\text{M}$; TCS-methyl: $1.0 \mu\text{M}$) and measuring the compound concentration after 48 h of agitation at 225 rpm. The influence of NaCl (ACS reagent, Sigma-Aldrich), phenol and humic acid (technical grade, Aldrich) on TCS sorption was studied by dosing 100 mg sorbents into 500 mL mixed solutions containing 1 mg L^{-1} TCS and a background compound. In a different set of control

experiments, the sorption of TCS in glass vessels, polypropylene sampling syringes and 0.2- μm RC filters (with first 2.0 mL filtrate disposed) was determined which verified negligible loss of TCS analyte during the entire sampling process.

Sorbent regeneration. Equilibrated solutions from sorption isotherm experiments were stored and sampled to analyze residual TCS concentrations in the solutions. The results were used to determine the total amount of TCS sorbed by sorbents thereby establish a basis to calculate the sorbent regeneration efficiency. TCS was desorbed from exhausted sorbents by hydrothermal treatment (at 75°C), alkaline elution (0.01–0.04 wt. % NaOH) and solvent elution (35–50 vol. % acetone), respectively. A maximum desorption period of 2 h was allowed for each desorption trial and the free TCS concentration was monitored in the regenerant solution during the desorption process.

Analytical method. TCS solutions were analyzed by high-performance liquid chromatography (HPLC) on a Shimadzu Prominence® HPLC system equipped with a UV detector. Triplicate measurements were performed for samples collected from single-concentration TCS sorption and desorption experiments to minimize measurement error. Analysis was performed at 205 nm wavelength using a C18 reverse-phase column (5 μm , 4.6 \times 150 mm, Agilent) with 2.5–50 μL sample injection. Acetonitrile (UV190, HPLC) and deionized water (18.2 M Ω -cm, Milli-Q) were mixed at 65:35 (v:v) and used as the mobile phase at a flow rate of 1.0 mL min⁻¹. The method yielded high signal-to-noise ratios and a detection limit <1 $\mu\text{g L}^{-1}$ for TCS in water.

Computational chemistry calculations. Quantitative structure–property relationship (QSPR) calculations were performed on the MARVIN® 5.9.3 Suite (ChemAxon) to determine molecule geometry, octanol-water partitioning coefficient, atomic charge and microspecies distribution. Quantum mechanical calculations were performed on the Gaussian® 03 program¹ to model the hydrogen bonding interactions between TCS and PA12 amide groups by calculating the bond distances and complexation energies of intermolecular hydrogen bonds between TCS, *N*-methylacetamide (NMA) and water molecules. Molecular conformation and equilibrium structures were optimized using the B3LYP exchange functional² and 6-31G+(d,p) basis sets. Single point energy calculations were performed on both B3LYP/6-31+G(d,p) and MP2/6-31+G(d,p) levels. Basis set superposition errors were estimated using counterpoise correction³ with the 6-31+G(d,p) basis set at both levels.

2. Description of the isotherm and kinetics models used in this study

Sorption isotherm data in this study were fit to the Langmuir and Freundlich isotherm models by linear regression method. The Langmuir and Freundlich isotherm models represent two of the most extensively adopted models for describing sorption phenomena in aqueous media. The Langmuir isotherm model is a theoretical equation based on the assumptions of limited sorption sites, monolayer sorption and reversible sorption at equilibrium. The model can be expressed as:

$$q_e = q_0 b C_e / (1 + b C_e)$$

or in its linear form,

$$C_e / q_e = 1 / q_0 b + (1 / q_0) C_e$$

where q_e (mg g^{-1}) represents the amount of solute sorbed by per unit weight of sorbent at equilibrium; C_e (mg L^{-1}) represents the equilibrium concentration of solute compound; q_0 (mg g^{-1}) represents the maximum sorption capacity of sorbent; and b ($\text{L}^{-1} \text{mg}$) is a constant indicative of binding energy. The parameters of the Langmuir isotherm model can be determined from the slope and intercept of the plot between C_e / q_e and C_e .

The Freundlich isotherm model is an empirical equation which can be expressed as:

$$q_e = K_f C_e^{1/n}$$

or in its linear form,

$$\log q_e = \log K_f + (1/n) \log C_e$$

q_e (mg g^{-1}) and C_e (mg L^{-1}) represent the same parameters as in Langmuir isotherm model. The Freundlich capacity factor K_f ($(\text{mg g}^{-1}) / (\text{mg L}^{-1})^{1/n}$) is a measure of sorption capacity, and the Freundlich intensity parameter $1/n$ (dimensionless) is indicative of the strength of sorptive interactions. The parameters of the Freundlich isotherm model can be determined from the slope and intercept of the plot between $\log q_e$ and $\log C_e$.

The pseudo-second order kinetics model is accurate for describing elementary reversible sorptive reactions on solid phases in aqueous media.⁴ The model can be expressed by the following equation,

$$t/q = 1/kq_e^2 + t/q_e$$

where t (min) is the sorption time; k ($\text{g mg}^{-1} \text{min}^{-1}$) is the sorption rate constant; q and q_e (mg g^{-1}) are the sorption capacity at a particular time (t) and sorption equilibrium, respectively. Detailed theoretical analysis and mathematical derivation of the model are available from literature.⁴

3. Figures

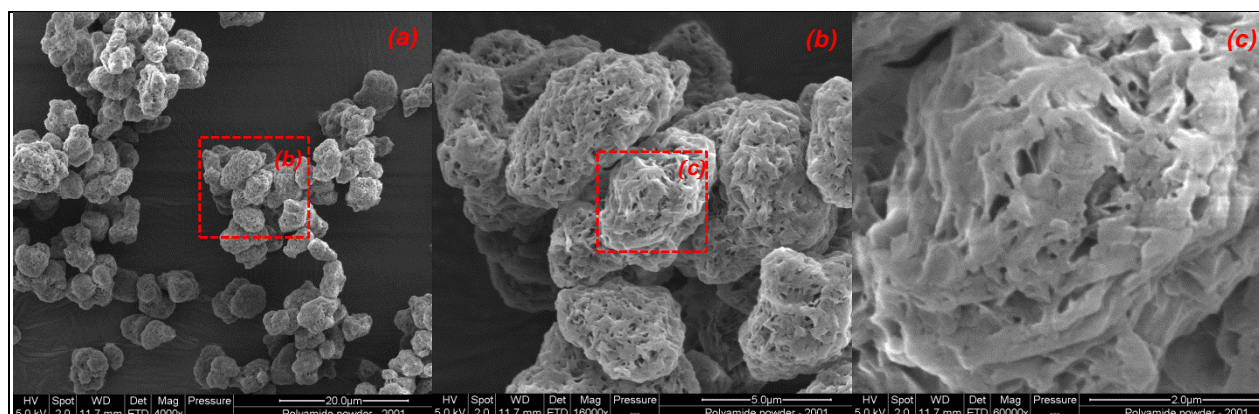


Fig. S1 Typical morphologies of PA12 microspheres observed under a scanned electron microscope

Discussion: The micrographs above show typical surface morphologies of PA12 microspheres used in this study. It can be seen that PA12 microspheres have a slightly roughened surface morphology, with submicro- to micro-sized cavities on their surfaces. These microspheres, although they may appear to be somewhat “porous” at first glance, are in fact nonporous as shown in Fig. S1c under a higher magnification. This is also evidenced by their low specific surface areas ($9.1 \text{ m}^2 \text{ g}^{-1}$), large cavity size (avg. 213 \AA), and negligible pore volume ($0.05 \text{ cm}^3 \text{ g}^{-1}$) compared to the real porous sorbent media, as determined by BET surface area measurements (Fig. 1). These measurements reflect the nature of the surface cavities on PA12 microspheres as opposed to a rich pore structure.

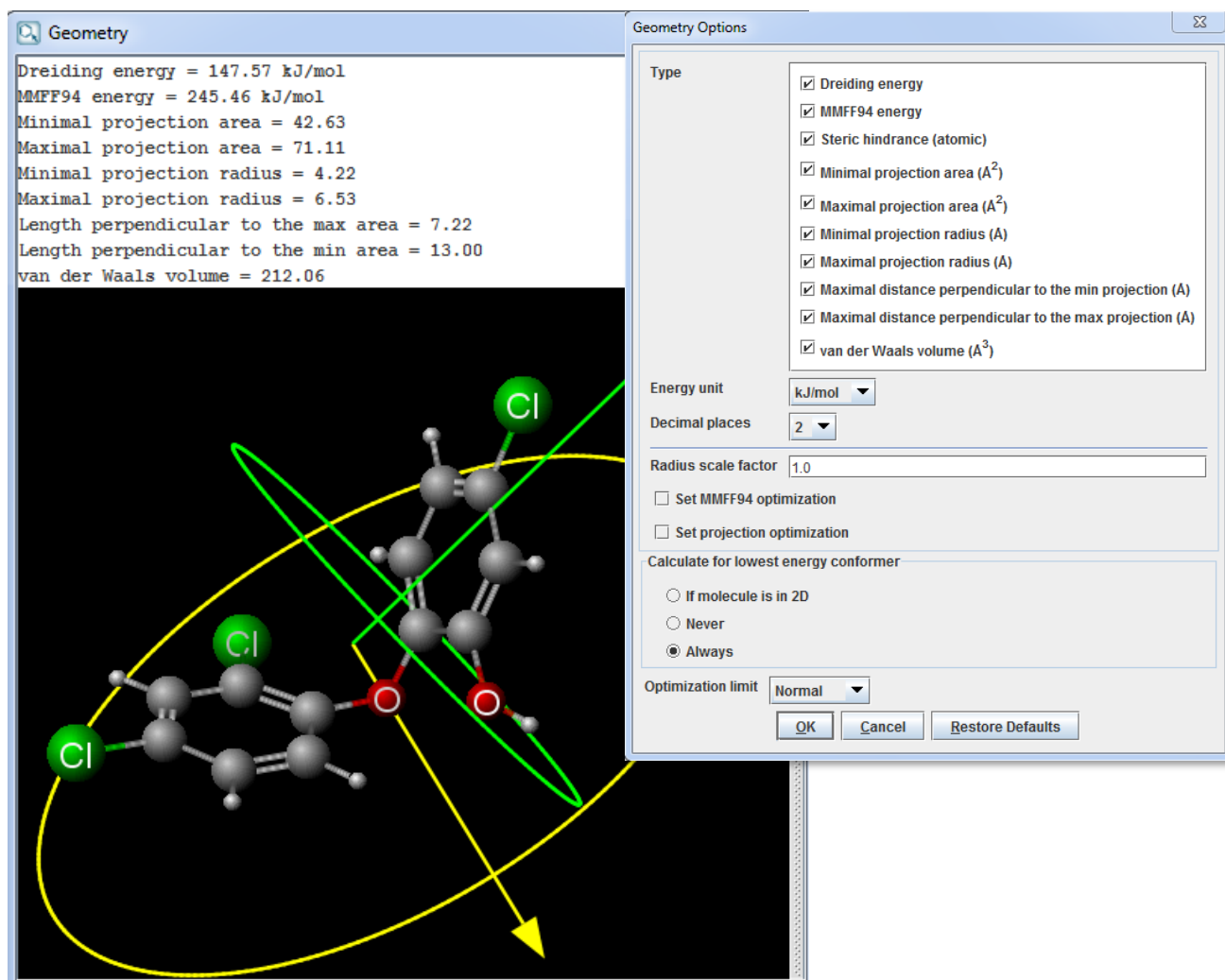


Fig. S2 TCS molecular geometry computed by MARVIN® 5.9.3 Suite. Image displays the lowest energy conformer of TCS molecule.

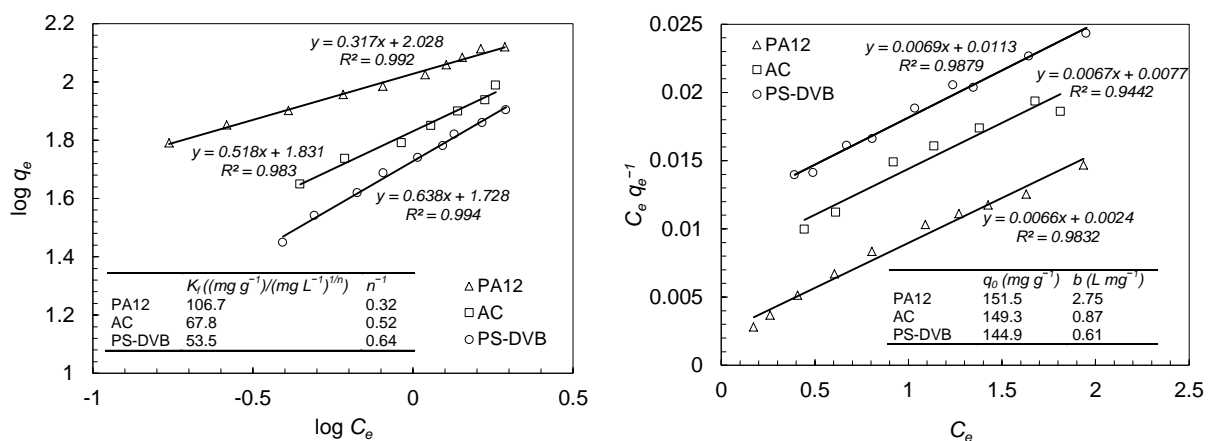


Fig. S3 Sorption isotherm of TCS on PA12, AC and PS-DVB in aqueous solutions. Data are fitted to Freundlich and Langmuir isotherm models. Sorbent dosage: 10 mg (dry weight basis), 200 mL; agitation: 225 rpm, 48 h; at 298 K. C_e (mg L^{-1}) represents TCS equilibrium concentration and q_e (mg g^{-1}) represents the corresponding sorption capacity.

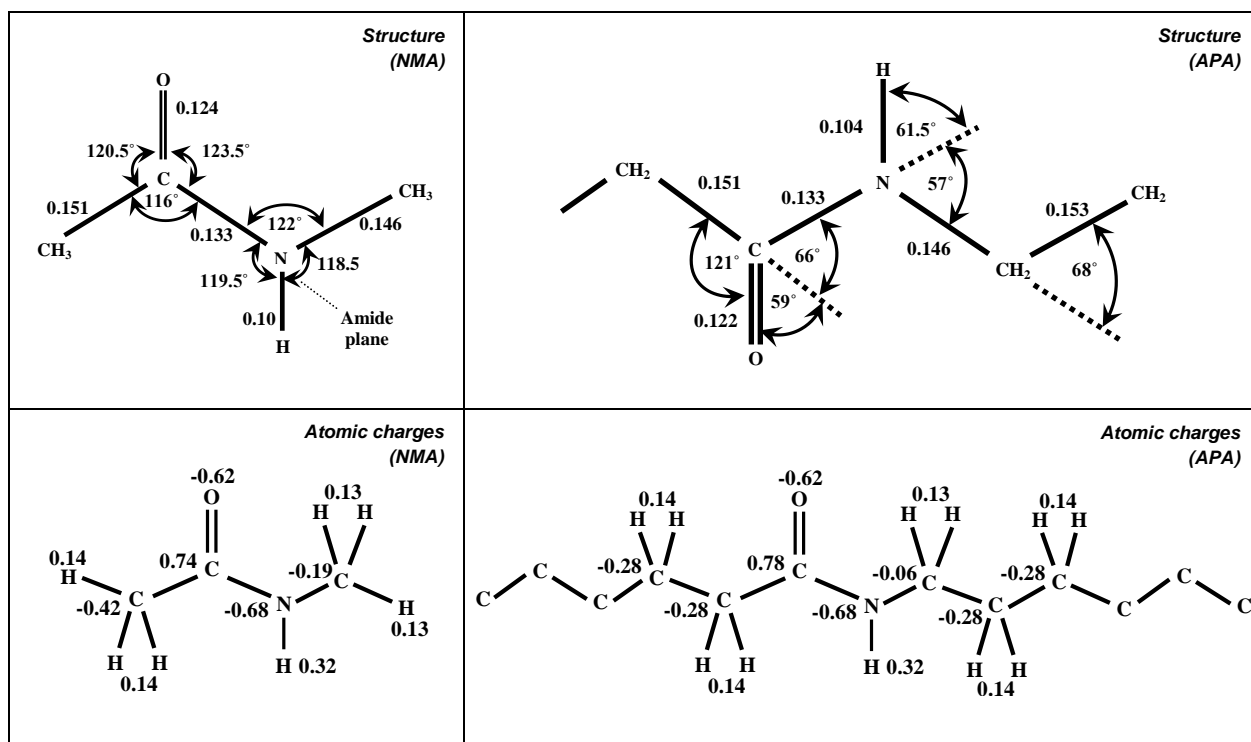


Fig. S4 Structures and atomic charges of amide groups in *N*-methylacetamide (NMA) and aliphatic polyamides (APA). After Dasgupta *et al.* ⁵; Mirkin and Krimm⁶.

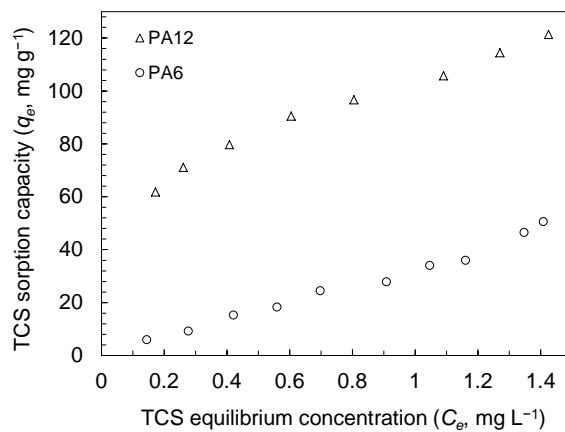


Fig. S5 Sorption isotherms of TCS on PA6 and PA12 microspheres in aqueous solutions. Sorbent dosage: 10 mg (dry weight basis), 200 mL; agitation: 225 rpm, 48 h; at 298 K.

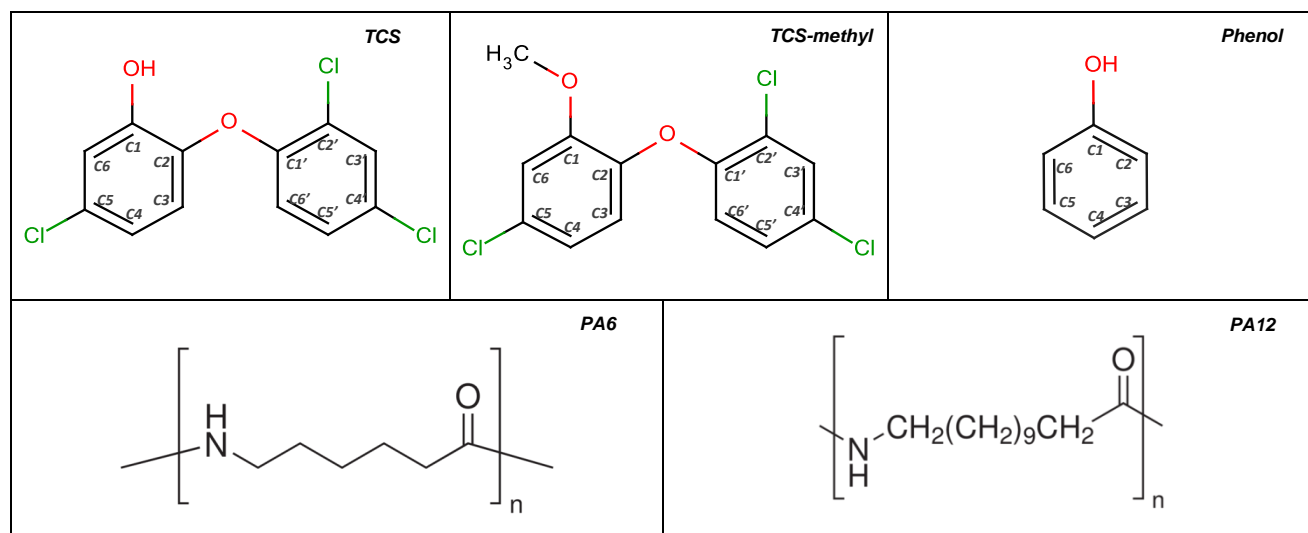


Fig. S6 Structural formula and atom numbering schemes of TCS, TCS-methyl and phenol molecules (above); chemical repeating unit in PA6 and PA12 (below).

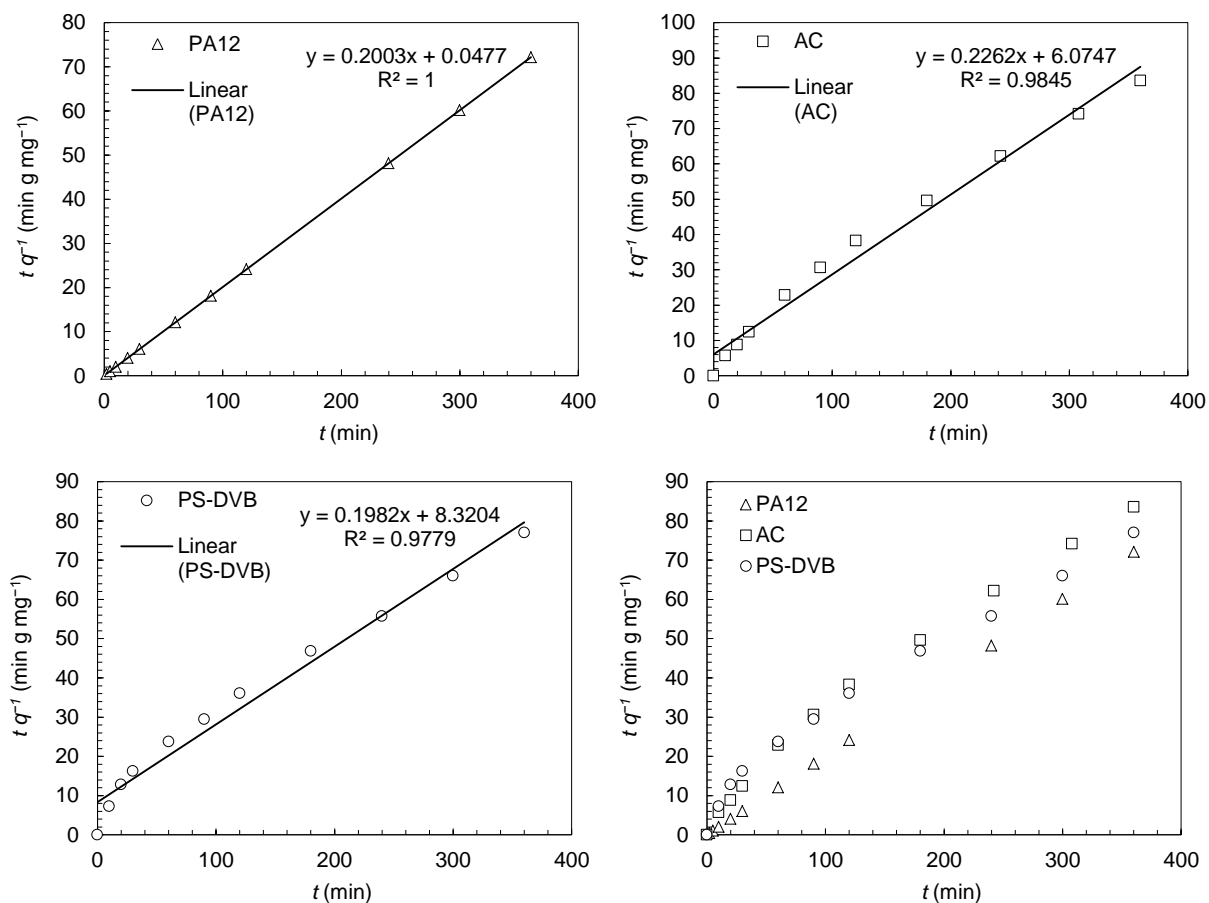


Fig. S7 Sorption kinetics of TCS by PA12, AC and PS-DVB in aqueous solutions. Sorption data are fitted to the pseudo second-order kinetics model. Initial TCS concentration: 1.0 mg L⁻¹; sorbent dosage: 100 mg (dry weight basis), 500 mL; agitation: 225 rpm; at 298 K.

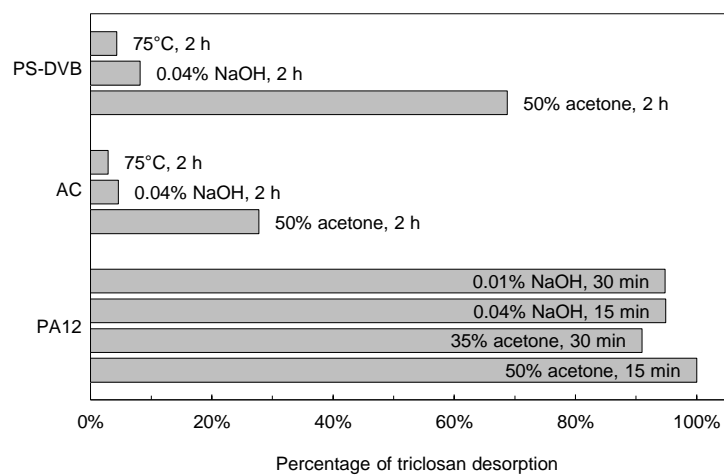


Fig. S8 Sorbent regeneration via hydrothermal treatment, alkaline elution and solvent elution

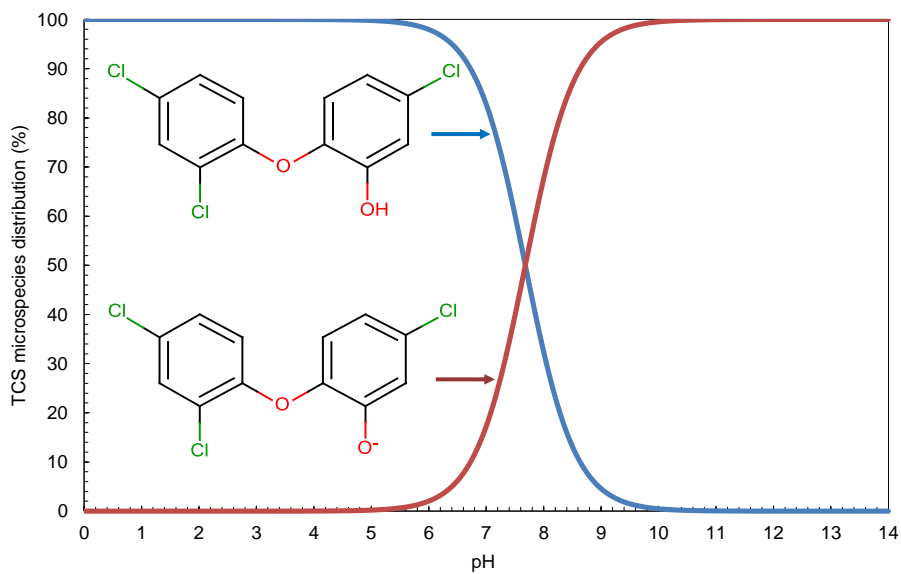
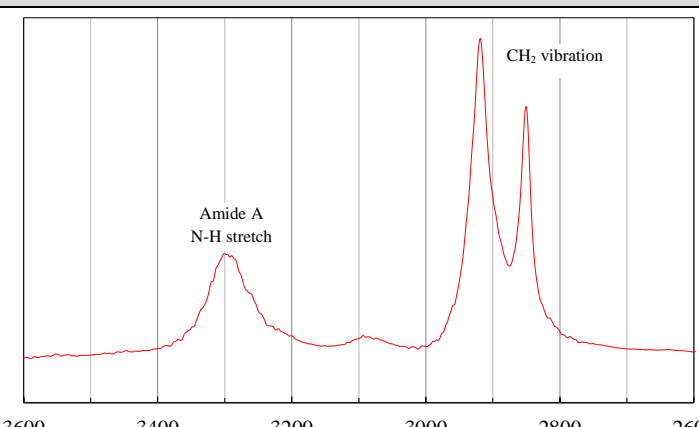
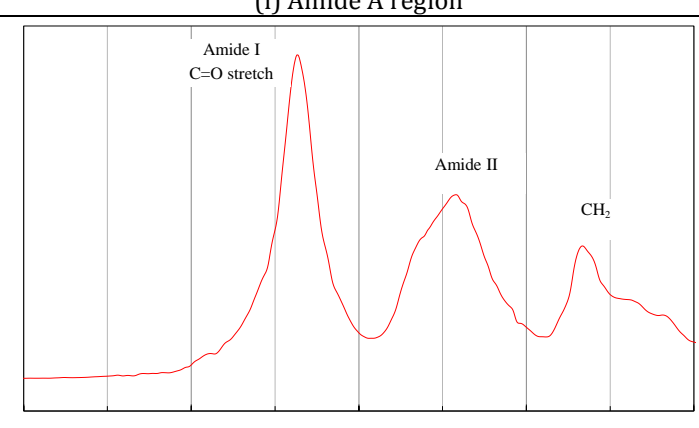
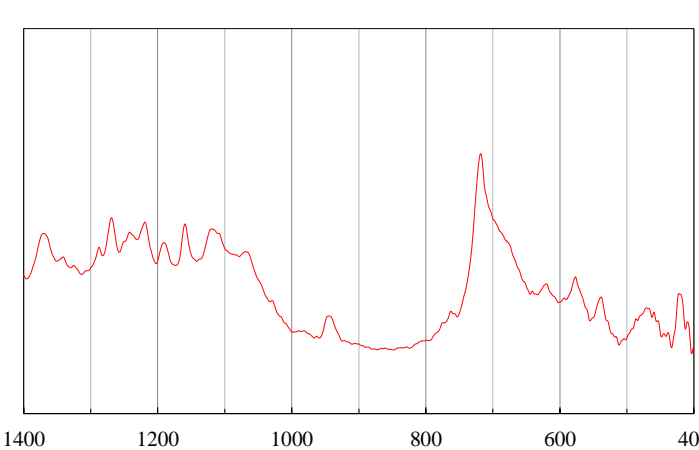


Fig. S9 Microspecies distribution of TCS solutes in water at different pH levels as predicted by calculations using MARVIN® 5.9.3 Suite

4. Tables

Table S1 ATR-FTIR spectrum of PA12 microspheres and comparison with standard PA12 spectral data

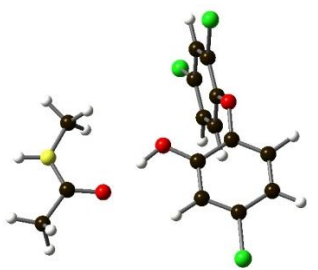
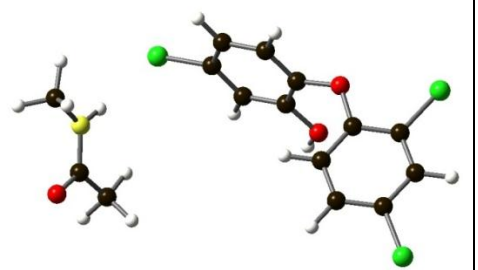
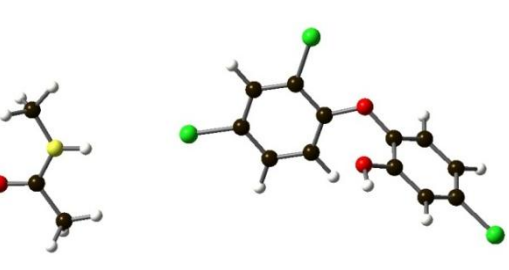
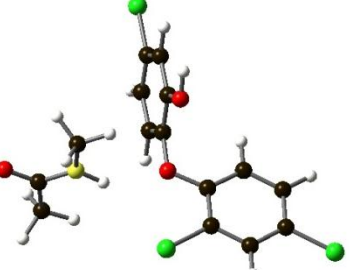
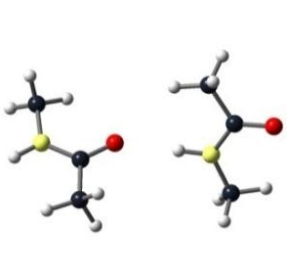
FTIR spectrum of PA12 microspheres	FTIR peaks (cm ⁻¹)	Standard PA12 FTIR peaks (cm ⁻¹)*	Peak assignments*
	3300	3320 (α-form) 3310 (γ-form)	Hydrogen-bonded N-H stretching
	3094	3080 (α-form) 3090 (γ-form)	Fermi-resonance of N-H stretching, with an overtone amide II
	2919	2930 (α-form) 2930 (γ-form)	CH ₂ asymmetric stretching
	2850	2860 (α-form) 2860 (γ-form)	CH ₂ symmetric stretching
(i) Amide A region			
	1636	1635 (α-form) 1640 (γ-form)	Amide I, C=O stretching
	1542	1540 (α-form) 1563 (γ-form)	Amide II, C-N stretching + C=O in plane bending
	1467	1470 (α-form) 1466 (γ-form)	N-vic. CH ₂ bend
(ii) Amide I and II region			
	1370	1370 (α-form) 1368 (γ-form)	CH bend, CH ₂ twisting
	1269	1272 (α-form) 1268 (γ-form)	Amide III (C-N stretching + C=O in plane bending)
	1159	1160 (α-form) 1160 (γ-form)	Skeletal motion involving CONH
	1119	1120 (α-form) 1122 (γ-form)	C-C stretching
	945	936 (α-form) 946 (γ-form)	CONH in plane
	718	720 (α-form) 721 (γ-form)	CH ₂ rocking
	624	627 (γ-form)	Amide VI, N-H out-of-plane bending
	577	578 (α-form)	Amide VI, N-H out-of-plane bending
(iii) Fingerprint region (1400–500 cm⁻¹)			

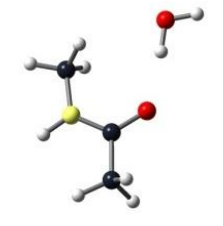
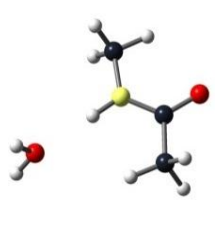
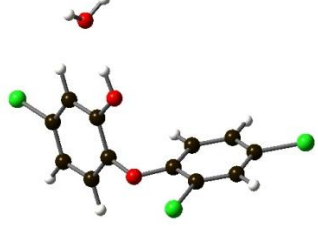
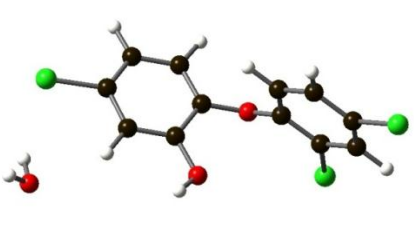
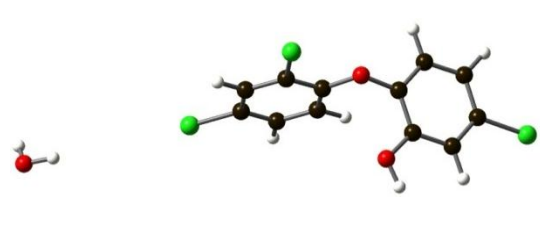
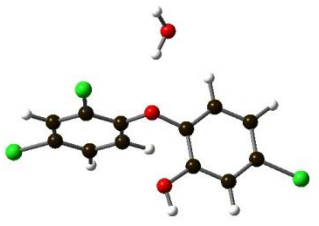
*More detailed IR band assignments available from literature.^{7,8} Minor variations exist in literature.

Table S2 Comparison with relevant literature data on the sorption capacity for TCS in water

Part I: Literature data - Synthetic sorbent materials, modelled by Langmuir isotherm model					
Sorbent material	Details of sorbent material	BET surface area (m² g⁻¹)	Maximum sorption capacity (q₀, mg g⁻¹)	Surface-normalized maximum sorption capacity (mg m⁻²)	Refs
PA12	PA12 microspheres	9.1	131.8 (experimentally obtained value); 151.5 (model derived maximum)	14.5 (experimentally obtained value); 16.6 (model derived maximum)	This work
AC	Activated carbon, charcoal based (DC Chemical Co, Korea)	739	18.5–70.4 (pH 3–10)	0.025–0.095	Behera <i>et al.</i> ⁹
Carbon nanotubes	Single-walled carbon nanotubes	1020	558.2 (at pH 7)	0.55	Cho <i>et al.</i> ¹⁰
	Multiwalled carbon nanotubes	283	434.7 (at pH 7)	1.54	
	Oxidized multiwalled carbon nanotubes	287	105.4 (at pH 7)	0.37	
Molecularly imprinted core-shell carbon nanotubes	Triclosan-imprinted core-shell carbon nanotubes	Not specified	2.941	-	Gao <i>et al.</i> ¹¹
	Non-imprinted core-shell carbon nanotubes	Not specified	0.957	-	
Part II: Literature data - natural sorbent materials, data modelled by Langmuir isotherm model					
Sorbent material	Details of sorbent material	BET surface area (m² g⁻¹)	Maximum sorption capacity (q₀, mg g⁻¹)	Surface-normalized maximum sorption capacity (mg m⁻²)	Refs
Montmorillonite	Montmorillonit, in the form of Bentonite, Yakuri Pure Chemicals Co., Japan	34.3	0.24–3.3 (at pH 3–10)	0.007–0.096	Behera <i>et al.</i> ⁹
Kaolinite	Junsei Chemical Co., Japan	2.3	4.95–22.02 (at pH 3–10)	2.15–9.57	
Sieved dry sediment particles	River sediments from 3 sites, containing clay (13%–26%), silt (15%–46%) and sand (27%–72%). Size ≤1.0 mm	583–704	0.261–0.285	<0.001	Lin <i>et al.</i> ¹²
Part III: Literature data - natural sorbent materials, data modelled by Freundlich isotherm model					
Sorbent material	Details of sorbent material	BET surface area (m² g⁻¹)	Comparison of equivalent sorption capacities		Refs
Sandy loam and silt loam soils	Sandy loam consisted of 74% sand, 10% silt and 16% clay. Silt loam consisted of 34% sand, 54% silt and 12% clay. Both were sieved (4 mm) prior to use.	Not specified	Sorption capacity of PA12: <i>ca.</i> 124 mg g ⁻¹ at C _e = 1.5 mg L ⁻¹ Equivalent sorption capacity: <i>ca.</i> 0.35–0.45 mg g ⁻¹ at C _e = 1.5 mg L ⁻¹ as graphically determined from the sorption data shown in the study.		Karnjanapi-boonwong <i>et al.</i> ¹³
Silt clay and sandy loam soils amended by biosolids	Silt clay and sandy loam soils. Air-dried, disaggregated, sieved (2 mm) and amended by biosolids	Not specified	Sorption capacity of PA12: 61.7 mg g ⁻¹ at C _e = 0.17 mg L ⁻¹ Equivalent sorption capacity: <0.04 mg g ⁻¹ at C _e = 0.17 mg L ⁻¹ as graphically determined from the sorption data shown in the study.		Wu <i>et al.</i> ¹⁴
Agricultural soils	Hanford loamy sand (HLS), Airlington sandy loam (ASL), Imperial silty clay (ISC) and Palouse silt loam (PSL).	Not specified	Sorption capacity of PA12: 61.7 mg g ⁻¹ at C _e = 0.17 mg L ⁻¹ Highest adsorption obtained with PSL. Equivalent sorption capacity: <0.02 mg g ⁻¹ at C _e = 0.17 mg L ⁻¹ as graphically determined from the sorption data shown in the study.		Xu <i>et al.</i> ¹⁵
Activated sludge	Activated sludge collected from a nitrifying zone of a municipal WWTP	Not specified	Sorption capacity of PA12: 131.8 mg g ⁻¹ at C _e = 1.94 mg L ⁻¹ Equivalent sorption capacity: 0.427 mg g ⁻¹ at C _e = 1.94 mg L ⁻¹ as extrapolated from the Freundlich isotherm established in the study, <i>i.e.</i> y=0.5543x+3.8084 where C _e is in μg L ⁻¹ and q _e is in μg Kg ⁻¹ (dry weight basis).		Wick <i>et al.</i> ¹⁶
Biosolids	Biosolids collected from 19 WWTPs in Australia	Not specified	Low sorption capacities: 0.09–16.79 μg g ⁻¹ on dry weight basis (median value: 2.32 μg g ⁻¹)		Kookana <i>et al.</i> ¹⁷

Table S3 Quantum mechanical modelling of the bond distances and energies of intermolecular hydrogen bonds in a ternary system consisting of NMA, TCS and H₂O molecules

H donor-acceptor	NMA-TCS				NMA-NMA
	CO(NMA)-HO(TCS)	NH(NMA)-Cl1(TCS)	NH(NMA)-Cl2(TCS)	NH(NMA)-Cl3(TCS)/O(TCS)	CO(NMA)-HN(NMA)
Molecular conformations					
Bond distance	1.709 Å	2.783 Å	3.458 Å	2.463 - 2.458 Å	1.993 Å
Complexation energy (ΔE) (B3LYP) (kJ mol ⁻¹)	-51.6876	-4.47679	-1.21171	-11.2759	-25.5027
Basis set superposition errors (BSSE) (kJ mol ⁻¹)	6.421589	1.048764	0.400331	2.516462	1.3267
Corrected complexation energy ($\Delta E'$) (B3LYP) (kJ mol ⁻¹)	-45.266	-3.42803	-0.81138	-8.75944	-24.1760
Complexation energy (ΔE) (MP2) (kJ mol ⁻¹)	-46.9544	-4.90056	-2.88518	-12.8299	-37.9123
Basis set superposition errors (BSSE) (kJ mol ⁻¹)	12.00997	7.18824	2.061276	15.47184	6.7096
Corrected complexation energy ($\Delta E'$) (MP2) (kJ mol ⁻¹)	-34.9444	2.28768	-0.8239	2.64194	-31.2027

H donor-acceptor	NMA-H ₂ O		H ₂ O-TCS			
	CO(NMA)-HO(H ₂ O)	NH(NMA)-OH(H ₂ O)	HO(H ₂ O)-HO(TCS)	OH(H ₂ O)-Cl1(TCS)	OH(H ₂ O)-Cl2(TCS)	OH(H ₂ O)-Cl3(TCS)/O(TCS)
Molecular conformations						
Bond distance (Å)	1.866 Å	2.056 Å	1.819 Å	2.695 Å	4.487 Å	2.121 Å
Complexation energy (ΔE) (B3LYP) (kJ mol ⁻¹)	-30.1307	-18.5192	-38.8755	-9.72731	-1.03103	-18.8809
Basis set superposition errors (BSSE) (kJ mol ⁻¹)	2.1124	3.4071	3.609647	1.903821	0.093405	5.18666
Corrected complexation energy ($\Delta E'$) (B3LYP) (kJ mol ⁻¹)	-28.0183	-15.1121	-35.2659	-7.82349	-0.93763	-13.6942
Complexation energy (ΔE) (MP2) (kJ mol ⁻¹)	-35.0029	-23.6311	-34.0521	-7.93816	-2.31746	-17.0328
Basis set superposition errors (BSSE) (kJ mol ⁻¹)	6.1028	7.7116	11.37989	5.927191	0.403468	11.95123
Corrected complexation energy ($\Delta E'$) (MP2) (kJ mol ⁻¹)	-28.9001	-15.9195	-22.6722	-2.01097	-1.91399	-5.08157

Notes:

1. Calculations were based on lowest energy conformers of molecules. C, N, O, H, Cl atoms are marked in black, yellow, red, white and green, respectively.
2. Calculations of complexation energies by the DFT-B3LYP method showed a higher degree of reliability for the ternary system.

Table S4 Effects of water chemistry constituents on the sorption of TCS by PA12, AC and PS-DVB

Water matrix constituents	Initial concentration ($\mu\text{g L}^{-1}$)	After sorption ^a ($\mu\text{g L}^{-1}$)		
		PA12	PS-DVB	AC
Blank (Milli-Q water)	1000	2.8 ± 0.1	8.0 ± 0.2	3.4 ± 0.1
NaCl 1M (60 g L^{-1})	1000	n.d.	n.d.	9.8 ± 0.4
Phenol (10 mg L^{-1})	1000	2.6 ± 0.3	9.5 ± 0.1	5.3 ± 0.2
Humic acid (0.5 mg L^{-1})	1000	3.4 ± 0.2	106.8 ± 1.3	117.7 ± 4.9

^aSorbent dosage: 100 mg (dry weight basis), 500 mL; agitation: 225 rpm, 48 h; at 298 K.

Table S5 Physicochemical properties of sorbent materials

Sorbent	Product name	Chemical composition	Morphology	BET surface area (m ² g ⁻¹)	Particle Size (mm)	Average pore size (nm)
Activated carbon (AC)	NORIT® 1240W ^a	Carbon, activated	Porous granules	989.2	0.6 - 0.7	3.2
Macroreticular polymeric sorbent resin (PS-DVB)	AMBERLITE™ XAD4 ^b	Divinylbenzene-crosslinked polystyrene	Porous macroreticular spheres	814.3	0.49 - 0.69	7.4
Aliphatic polyamides (PA)	ORGASOL® 2001 ^c	Polyamide 12	Nonporous microspheres	9.1	0.005 ± 0.001 (5 ± 1 μm)	Nonporous
	Toray® TR1 ^d	Polyamide 6	Nonporous microspheres	2.8	0.013 (13 μm)	Nonporous

^aNorit Netherlands B.V., Datasheet - Norit GAC 1240W, Document No. 124WD, 25 May 2011

^bRohm and Haas Company, AMBERLITE™ XAD4 Industrial Grade Polymeric Adsorbent, Jun 2001.

^cArkema Inc., Orgasol® Polyamide Powders - General Bulletin. www.arkema-inc.com/literature/pdf/91.pdf (Accessed on Nov 24, 2012)

^dKobo Products Inc., Polymer microspheres. www.koboproductsinc.com/Microspheres.html (Accessed on Nov 24, 2012)

References

1. Frisch, M. J., Trucks, G. W., Schlegel, H. B., Scuseria, G. E., Robb, M. A., Cheeseman, J. R., Montgomery, J. J. A., Vreven, T., Kudin, K. N., Burant, J. C., Millam, J. M., Iyengar, S. S., Tomasi, J., Barone, V., Mennucci, B., Cossi, M., Scalmani, G., Rega, N., Petersson, G. A., Nakatsuji, H., Hada, M., Ehara, M., Toyota, K., Fukuda, R., Hasegawa, J. I. M., Nakajima, T., Honda, Y., Kitao, O., Nakai, H., Klene, M., Li, X., Knox, J. E., Hratchian, H. P., Cross, J. B., Bakken, V., Adamo, C., Jaramillo, J., Gomperts, R., Stratmann, R. E., Yazyev, O., Austin, A. J., Cammi, R., Pomelli, C., Ochterski, J. W., Ayala, P. Y., Morokuma, K., Voth, G. A., Salvador, P., Dannenberg, J. J., Zakrzewski, V. G., Dapprich, S., Daniels, A. D., Strain, M. C., Farkas, O., Malick, D. K., Rabuck, A. D., Raghavachari, K., Foresman, J. B., Ortiz, J. V., Cui, Q., Baboul, A. G., Clifford, S., Cioslowski, J., Stefanov, B. B., Liu, G., Liashenko, A., Piskorz, P., Komaromi, I., Martin, R. L., Fox, D. J., Keith, T., Al-Laham, M. A., Peng, C. Y., Nanayakkara, A., Challacombe, M., Gill, P. M. W., Johnson, B., Chen, W., Wong, M. W., Gonzalez, C. and Pople, J. A., Gaussian 03, Revision C.02, Gaussian, Inc., Wallingford CT, 2004.
2. Becke, A. D., Density-functional thermochemistry. *Abs. Pap. Am. Chem. Soc.* 212 (1996) 112-COMP.
3. Herrebout, W. A., Clou, K. and Desseyn, H. O., Vibrational spectroscopy of N-methylacetamide revisited. *J. Phys. Chem. A*, 105 (2001) 4865-4881.
4. Azizian, S., Kinetic models of sorption: A theoretical analysis. *J. Colloid Interf. Sci.* 276 (2004) 47-52.
5. Dasgupta, S., Hammond, W.B., Goddard W.A., III. Crystal structures and properties of nylon polymers from theory, *J. Am. Chem. Soc.* 118 (1996) 12291-12301.
6. Mirkin, N.G. and Krimm, S., Ab Initio vibrational analysis of hydrogen-bonded *trans*- and *cis*-N-methylacetamide. *J. Am. Chem. Soc.* 113 (1991) 9742-9747.
7. S. Rhee and J.L. White, Crystal structure and morphology of biaxially oriented polyamide 12 films, *J. Polym. Sci. B*, 40 (2002) 1189-1200.
8. I. Matsubara, Y. Itoh and M. Shinomiya, Lower-frequency infrared spectrum (800-200 cm⁻¹) and structures of polyamides, *J. Polym. Sci. B*, 1966, 4, 47.
9. Behera, S. K., Oh, S.-K., Park, H.-S., Sorption of triclosan onto activated carbon, kaolinite and montmorillonite: Effects of pH, ionic strength, and humic acid, *J. Hazard. Mater.* 179 (2010) 684-691.
10. Cho, H.-H., Huang H. and Schwab, K., Effects of Solution Chemistry on the Adsorption of Ibuprofen and Triclosan onto Carbon Nanotubes, *Langmuir* 27 (2011) 12960-12967.
11. Gao, R.X., Kong, X.A., Su, F.H., He X.W., Chen, L.X. and Zhang, Y.K., Synthesis and evaluation of molecularly imprinted core-shell carbon nanotubes for the determination of triclosan in environmental water samples, *J. Chromatogr. A*, 1217 (2010) 8095-8102.
12. Lin, H., Hu, Y.-Y., Zhang, X.-Y., Guo Y.-P. and Chen G.R., Sorption of triclosan onto sediments and its distribution behavior in sediment-water-rhamnolipid systems, *Environ. Toxicol. Chem.* 30 (2011) 2416-2422.
13. Karnjanapiboonwong, A., Morse, A.N., Maul, J.D. and Anderson, T.A., Sorption of estrogens, triclosan, and caffeine in a sandy loam and a silt loam soil, *J. Soils Sediments*, 10 (2010) 1300-1307.
14. Wu, C., Spongberg, A.L. and Witter, J.D., Adsorption and Degradation of Triclosan and Triclocarban in Solis and Biosolids-Amended Soils, *J. Agric. Food Chem.*, 57 (2009) 4900-4905.
15. Xu, J., Wu, L. and Chang A.C., Degradation and adsorption of selected pharmaceuticals and personal care products (PPCPs) in agricultural soils, *Chemosphere*, 77 (2009) 1299-1305.
16. Wick, A., Marincas, O., Moldovan, Z. and Ternes, T.A., Sorption of biocides, triazine and phenylurea herbicides, and UV-filters onto secondary sludge, *Water Res.*, 45 (2011) 3638-3652.
17. Kookana, R.S., Ying G.-G. and Waller N.J., Triclosan: its occurrence, fate and effects in the Australian environment, *Water Sci. Technol.* 63 (2011) 598-604.